NeuroImage: Clinical 32 (2021) 102821

Contents lists available at ScienceDirect

NeuroImage: Clinical

journal homepage: www.elsevier.com/locate/ynicl

Neural correlates associated with impaired global motion perception in cerebral visual impairment (CVI)

Zahide Pamir [a,1], Corinna M. Bauer [a,1], Emma S. Bailin [a], Peter J. Bex [b], David C. Somers [c], Lotfi B. Merabet [a,*]

[a] The Laboratory for Visual Neuroplasticity, Department of Ophthalmology, Massachusetts Eye and Ear, Harvard Medical School, Boston, MA, USA
[b] The Translational Vision Laboratory, Department of Psychology, Northeastern University, Boston, MA, USA
[c] The Neuroimaging, Perception & Attention Laboratory, Department of Psychological & Brain Sciences, Boston University, Boston, MA, USA

ARTICLE INFO

Keywords:
Cerebral visual impairment
Global motion processing
Optic flow
fMRI
Diffusion imaging
Dorsal stream
Surround suppression

ABSTRACT

Cerebral visual impairment (CVI) is associated with a wide range of visual perceptual deficits including global motion processing. However, the underlying neurophysiological basis for these impairments remain poorly understood. We investigated global motion processing abilities in individuals with CVI compared to neurotypical controls using a combined behavioral and multi-modal neuroimaging approach. We found that CVI participants had a significantly higher mean motion coherence threshold (determined using a random dot kinematogram pattern simulating optic flow motion) compared to controls. Using functional magnetic resonance imaging (fMRI), we investigated activation response profiles in functionally defined early (i.e. primary visual cortex; area V1) and higher order (i.e. middle temporal cortex; area hMT+) stages of motion processing. In area V1, responses to increasing motion coherence were similar in both groups. However, in the CVI group, activation in area hMT+ was significantly reduced compared to controls, and consistent with a surround facilitation (rather than suppression) response profile. White matter tract reconstruction obtained from high angular resolution diffusion imaging (HARDI) revealed evidence of increased mean, axial, and radial diffusivities within cortico-cortical (i.e. V1-hMT+), but not thalamo-hMT+ connections. Overall, our results suggest that global motion processing deficits in CVI may be associated with impaired signal integration and segregation mechanisms, as well as white matter integrity at the level of area hMT+.

1. Introduction

Cerebral visual impairment (also referred to as cortical visual impairment, or CVI) has been defined as verifiable visual dysfunction associated with damage to retrochiasmatic pathways and cerebral structures that cannot be attributed to disorders of the anterior visual pathways or potentially co-occurring ocular pathology (Sakki et al., 2018). As the leading individual cause of pediatric visual impairment in developed countries (Solebo et al., 2017), CVI represents an important public health concern. However, the neurophysiological basis of visual processing deficits related to this condition, and their association with early neurological injury, remain poorly understood.

In the clinical setting, individuals with CVI typically present with a wide range of visual impairments including reduced visual acuity and contrast sensitivity, along with ocular motor deficits and visual field restriction (commonly within the inferior hemi-field) (Fazzi et al., 2007; Philip and Dutton, 2014). Even in the case where visual acuity and visual field functions are within normal range, deficits with higher order visuospatial processing (including the perception of complex motion) are also frequently observed which can have a profound impact on an individual's functioning and independence (Dutton et al., 2006; Boot et al., 2010; Dutton, 2013). Indeed, individuals with CVI often report feeling overwhelmed in crowded environments, and have difficulty walking down stairs or following the flow of moving traffic (Lam et al., 2010; McDowell and Dutton, 2019). These visual impairments are thought to be linked to the timing, location, and severity of the underlying neurological injury (Anderson et al., 2011) that affect the development of key visual processing networks within the brain (Volpe, 2009). Given the profile of these higher order visual deficits, and the role played by the dorsal visual stream in visuospatial and global motion

* Corresponding author.
E-mail address: lotfi_merabet@meei.harvard.edu (L.B. Merabet).
[1] Equal contributing first authors.

https://doi.org/10.1016/j.nicl.2021.102821
Received 7 April 2021; Received in revised form 7 August 2021; Accepted 7 September 2021
Available online 21 September 2021

processing, CVI has been characterized as "dorsal stream dysfunction" (Dutton, 2009; Macintyre-Beon et al., 2010); see also "dorsal stream vulnerability"; (Braddick et al., 2003).

The steps related to the analysis and integration of complex motion signals have been studied extensively in humans and animal models. Beginning at primary visual cortex (V1), local motion signals are detected and subsequently integrated into coherent, global percepts at the level of the middle temporal (MT/V5) area (or more accurately, the hMT+ complex which includes the medial superior temporal area; MST) (Tootell et al., 1995; Braddick et al., 2001). Evidence suggests that direction-selective neurons within area hMT+ respond more strongly to coherent than non-coherent motion (Previc et al., 2000; see also Ajina et al., 2015a). Furthermore, this area also exhibits a surround suppression effect (i.e. reduced activation) in response to visual stimuli that are larger than the size of the classical receptive field (cRF). With respect to motion processing, this latter property appears to be an important neural mechanism implicated in the processing of optic flow information (Cui et al., 2013) as well as segregating of moving objects from their backgrounds (Tadin et al., 2019), computing heading direction (Royden, 2002), and identifying the three-dimensional shape of moving objects (Buracas and Albright, 1996).

In light of the key role played by area hMT+, it would be reasonable to postulate that global motion perception deficits in CVI would be associated with impaired function within this region. Furthermore, in the setting of early neurological injury, we would also expect evidence of impaired structural connectivity along the dorsal visual pathway. In this study, we investigated global motion perception abilities in CVI by assessing psychophysical coherence thresholds and compared performance with individuals with neurotypical development. Given the nature of reported visuospatial impairments in CVI, we focused on perceptual abilities related to complex movement within a visual scene. Thus, in contrast to previous studies using visual stimuli such as sinusoidal gratings or random dot kinematogram (RDK) patterns with translational or rotational (circular) motion (e.g. MacKay et al., 2005; Guzzetta et al., 2009; Taylor et al., 2009, Weinstein et al., 2012#150; Bhat et al., 2021), we used an RDK pattern simulating optic flow (i.e. radial motion) as this stimulus is believed to mimic flow field motion associated with self-movement (egomotion) through the environment (Durant and Zanker, 2012). We then carried out an fMRI study to investigate the neural correlates related to global motion processing. Specifically, we explored the relationship between fMRI signal response profiles with respect to varying motion coherence levels focusing our attention on the relative contributions of cortical areas V1 and hMT+. As hMT+ is part of the dorsal visual processing pathway, the presence of an aberrant response profile in this region may also serve as a neurophysiological marker for dorsal stream dysfunction. This was followed by a detailed reconstruction and analysis of white matter tracts obtained by high angular resolution diffusion imaging (HARDI). For this component of the study, we focused on investigating the structural integrity between functionally-defined cortical areas V1 and hMT+ and between visual thalamic nuclei and hMT+ as indexed by tract volume and quantitative anisotropy (QA), along with mean, axial, and radial diffusivities (MD, AD, and RD respectively). Finally, we explored potential relationships between behavioral performance, fMRI response profiles, and white matter structural connectivity.

We hypothesized that as a group, CVI participants would show an impairment in global motion processing compared to controls as reflected by a higher motion coherence threshold in response to viewing the RDK optic flow stimulus. Furthermore, and in line with the dorsal stream dysfunction hypothesis, this behavioral deficit would be associated with impaired function and structural connectivity at the level of area hMT+. Specifically, we postulated that area hMT+ (but not V1) would show an aberrant response profile, along with evidence of reduced white matter integrity within cortico-cortical (i.e. V1-hMT+) as opposed to thalamo-cortical pathways implicated with motion processing.

2. Methods

2.1. Study participants

A total of 30 individuals participated in the study including 12 previously diagnosed with CVI (7 males, mean age = 17.36 years ± 3.03 SD). Eighteen (18) individuals with neurotypical development (9 males, mean age = 19.26 years ± 3.19 SD) served as comparative controls. There was no statistically significant difference between the groups with respect to age ($t = 1.59$, $df = 21.33$, $p = 0.13$). Control participants had normal or corrected to normal visual acuity and no previous history of ophthalmic (i.e. strabismus, amblyopia) or neurodevelopmental (e.g. epilepsy, attention deficit disorder) conditions. For the participants with CVI, all had visual impairments related to perinatal neurological injury, with an approximately equal distribution of individuals with periventricular leukomalacia (PVL) and non-PVL associated causes. Best corrected visual acuity ranged from 20/15 to 20/100 (Snellen equivalent; in the better seeing eye). Participants were required to have visual acuity sufficient to reliably fixate and perceive the relative motion of the RDK target, ocular motor fixation sufficient to perform the behavioral task, and intact visual field function within the area corresponding to the visual stimulus presentation. Exclusion criteria included any evidence of oculomotor apraxia, intraocular pathology (other than mild optic atrophy), and uncontrolled epilepsy. A full list of participant details can be found in Table 1.

All diagnoses of CVI were made by experienced eye care providers specializing in neuro-ophthalmic pediatric care. This was based on extensive review of medical records including neuroimaging and clinical electrophysiology findings, and reports from various allied providers (such as teachers of the visually impaired as well as occupational, physical and language therapists). A directed and objective assessment of visual function (e.g. visual acuity, contrast, perimetry, color) as well as thorough refractive and ocular examination was carried out. Further input regarding visual behaviors was drawn from a series of parent based questionnaires and inventories.

Participants with CVI were categorized into three groups (based on (Dutton and Lueck, 2015)): (1) "profound visual impairment due to CVI" (i.e. individuals using nonvisual approaches for learning needs, or have only rudimentary visual function), (2) "have functionally useful vision and cognitive challenges" (i.e. typically associated with widespread damage to the brain affecting vision and other functions including mobility) and, (3) "functionally useful vision and who can work at or near expected academic level for their age group" (i.e. the least severely affected, and with visual impairments typically associated with perceptual processing deficits).

Structural MRIs from CVI participants were assessed for brain lesion severity according to a reliable and validated semi-quantitative scale. The scoring procedure has been described in detail elsewhere (Fiori et al., 2014). Briefly, raw scores for each brain structure (lobe, subcortical structures, corpus callosum, and cerebellum) are calculated and summed to provide a global score, whereby a higher score is indicative of a greater degree of brain injury (representative images from CVI participants are shown in supplemental Fig. 1).

A subgroup of 21 participants (10 CVI, 11 controls) further participated in the functional imaging component of the study. Two participants with CVI who completed the behavioral task were excluded from the MRI experiment due to contraindications related to safety, and fMRI data from one participant with CVI were excluded due to excessive head motion (defined as more than one voxel size; i.e. 3 mm). Nineteen (19) participants participated in the diffusion based imaging component of the study. Data were excluded from one CVI participant due to extraneous motion, two control participants due to extraneous drift in the z-direction, and from one control participant due to a fat saturation artifact.

Written informed consent was obtained from all the participants and a parent/legal guardian (in the case of a minor) prior to commencing the

Table 1
CVI Participant Demographics.

CVI Participants	Sex	Age	Associated Cause of CVI	Preterm/ Term	CVI Classification	Distance Visual Acuity OD - OS (Snellen)	Distance Visual Acuity OD - OS (LogMar equivalent)	Motion Coherence Threshold
1	female	19	seizure disorder	term	2	20/20 - 20/30	0.0 - 0.2	N/A
2	female	17	meningitis, infarct	term	3	20/50 - 20/60	0.4 - 0.5	25.5
3	female	14	periventricular leukomalacia, infection	preterm	3	20/100 - 20/100	0.7 - 0.7	52.1
4	male	18	decreased placental perfusion	preterm	2	20/25 - 20/25	0.1 - 0.1	74.0
5	male	24	periventricular leukomalacia	preterm	2	20/80 - 20/80	0.6 - 0.6	42.2
6	male	16	periventricular leukomalacia	preterm	3	20/25 - 20/25	0.1 - 0.1	25.2
7	female	21	periventricular leukomalacia	preterm	2	20/50 - 20/40	0.4 - 0.3	66.8
8	female	16	complication related to birth	term	3	20/15 - 20/15	- 0.1 - -0.1	18.6
9	male	16	focal cortical atrophy, seizure disorder	term	3	20/60 - 20/60	0.5 - 0.5	18.1
10	male	14	genetic	term	3	20/20 - 20/20	0.0 - 0.0	22.4
11	male	15	infection	term	2	20/25 - 20/25	0.1 - 0.1	65.6
12	male	20	periventricular leukomalacia	preterm	3	20/40 - 20/25	0.3 - 0.1	75.5

study. The study was approved by the Investigative Review Board at the Massachusetts Eye and Ear in Boston, MA, USA and carried out in accordance to the Code of Ethics of the World Medical Association (Declaration of Helsinki) for experiments involving humans.

2.2. Visual stimulus and behavioral testing

Global motion processing was assessed by measuring an individual's motion coherence threshold in response to binocular viewing of an RDK stimulus pattern simulating optic flow. The stimulus was comprised of a set of coherently moving dots presented among an array of randomly moving noise dots (i.e. array of 200 black and white dots; mean luminance of 1 and 150 cd/m^2 respectively, dot diameter of 0.15°, with a grey background of 75 cd/m^2 luminance) subtending an area of 18.45° in diameter. The dots moved either inwards (contraction) or outwards (expansion) from the center of the screen and at varying levels of coherence on every trial following a 3-up, 1-down staircase procedure with a step size of 1 dB (1/20 log unit; (Wetherill and Levitt, 1965)). The direction and speed of each dot was calculated from the orientation (θ) and eccentricity (ε) of its center relative to the center of the display area calculated as:

$$\theta = atan2((y_{dot} - y_{screen}), (x_{dot} - x_{screen})) \quad (1)$$

$$\varepsilon = \sqrt{(y_{dot} - y_{screen})^2 + (x_{dot} - x_{screen})^2} \quad (2)$$

The direction of motion for each dot (Θ) differed for signal and noise dots. Noise dots were assigned a random direction drawn from a uniform distribution in the interval (-π, π) radians. The direction of each signal dot was dependent on its orientation with respect to the center of the screen: for expansion, Θ = θ (from equation (1)); for contraction, Θ = θ + π. The speed of signal and noise dots, (*s*) varied with eccentricity (ε from equation (2)) as 0.5ε per second. (As a comparison, for clockwise (Θ = θ + π/2) or counter-clockwise (Θ = θ-π/2) rotational motion, this would correspond to 0.5 rotations per second). Horizontal (δ_x) and vertical (δ_y) displacements each frame for both signal and noise dots were calculated as:

$$\delta_x = cos(\Theta)^* \frac{0.5\varepsilon}{F} \quad (3)$$

$$\delta_y = sin(\Theta)^* \frac{0.5\varepsilon}{F} \quad (4)$$

where F is the monitor frame rate in Hz. Any dots that moved outside the display area were assigned a new random location within the display area. To prevent tracking of individual dots, the lifetime of each dot was limited to 100 ms (6 video frames on our 60 Hz system) after which it was repositioned to a new random location within the display area. Each dot was assigned a random starting age, drawn from a uniform distribution in the interval (1, 6) frames to prevent all dots expiring simultaneously.

Participants were seated comfortably in front of a 14 in. (35 cm) computer monitor (viewing distance of 40 cm) and were instructed to identify the direction of motion (two-alternative forced-choice design) by responding verbally or by touching the designated side corresponding to the direction of motion. For the purposes of this experiment, reaction times were not recorded because of potential differences between participants responding verbally compared to touching the screen. The coherence level of the stimulus in each trial was manipulated adaptively with a 3-down 1-up staircase procedure. The staircase was terminated either after 8 reversals or 50 trials, whichever was completed first. An individual's motion coherence threshold was calculated by finding the proportion of dots (expressed as a percentage) moving coherently such that the participant correctly identified the direction of motion with a 79% success rate.

Group differences in motion coherence thresholds between CVI and controls were evaluated using a nonparametric independent-samples Mann-Whitney *U* test. Statistical analyses were performed using the SPSS Version 24 package (SPSS Inc., Chicago, IL).

2.3. MRI data acquisition

Participants underwent an MRI scanning protocol using a 3 T Philips Intera Achieva system and a 32-channel phased array head coil. Structural data were acquired using a high resolution T1-weighted structural image sequence (TE 3.1 ms, TR 6.7 ms, flip angle 9°, 0.98 × 0.98 × 1.20 mm voxel size). Blood oxygen level dependent (BOLD) signal measurements were acquired using a protocol based on a multi-slice fast field (gradient) echo-planar imaging (EPI) and standard parameters (TE 28 ms, TR 2000 ms, flip angle 90°, isotropic 3 mm voxel size, oriented axially, and covering the whole brain). A separate protocol was used for the purposes of the diffusion based imaging component. Specifically, an 8-channel phased array head coil was used to acquire two structural T1-weighted scans using a turbo spin echo sequence (TE = 3.1 ms, TR = 6.8 ms, flip angle = 9°, voxel size 0.98 × 0.98 × 1.20 mm, no slice gap, acquisition matrix 256 × 254). Diffusion based imaging was carried out using high angular resolution diffusion imaging (HARDI). Images were acquired with a single-shot EPI sequence (TE = 73 ms, TR = 17844 ms,

flip angle 90°, 64 directions, EPI factor = 59, B0 = 0 s/mm^2, Bmax = 3000 s/mm^2, acquired voxel size = 2 mm isotropic, reconstructed voxel size 1.75 × 1.75 × 2.00 mm, no slice gap, enhanced gradients at 66 mT/m, and a slew rate of 100 T/m/ms).

2.3.1. Functional MRI (fMRI) task and data analysis

The fMRI experiment followed a block-design consisting of five conditions. Three conditions included the RDK optic flow stimulus at fixed coherence levels: 0% (random motion; no coherence), 30% (below the CVI and above the control group threshold; based on behavioral testing), and 100% (full coherence; supra-threshold). "Twinkle" (flashing static dots, no motion) and rest (only a fixation point visible) conditions were also included as comparators. The twinkle condition served to control for the effect of local motion energy. The RDK stimulus was the same used in the behavioral experiment except with a stimulus size subtending 21.3° in diameter and back projected onto a translucent screen using a video projector (NEC MT1050NL). Participants could see the screen via an overhead mirror located above their eyes and attached to the head coil (viewing distance of 122 cm). Each condition was presented for 16 sec and repeated 4 times for a total run length of 5 min and 20 sec. Motion direction was reversed every 2 sec to avoid visual stimulus adaptation. Two different run sequences were generated using a pseudo-randomized order and each was repeated twice for a total of 4 runs. The same presentation order was used for each participant and most participants completed all runs (3 CVI subjects were not able to complete all four runs due to visual fatigue). Participants were instructed to fixate a central fixation point at the center of the RDK stimulus. During the task, the central fixation point briefly changed color (from white to red) at random intervals. Participants were instructed to press a button key when they noticed the color change to maintain attentiveness throughout the task. The size of the fixation point was adjusted as needed to ensure that it was visible for each participant.

Region of Interest (ROI) analysis: Structural and functional data were preprocessed and analyzed using BrainVoyager software Version 20.4 (Brain Innovation, The Netherlands). T1-weighted structural images were *iso*-voxelled (1 × 1 × 1 mm) and corrected for inhomogeneities and transformed into the AC-PC plane. Preprocessing steps for the functional images included three-dimensional head motion correction, high-pass temporal filtering, and slice scan time correction. Functional images were aligned with the structural image for each subject using a gradient-based affine alignment. Given the known inter-individual variability in localizing area hMT+, one of the functional runs was selected randomly for each participant and used as a functional localizer to identify voxels more responsive to moving stimuli (Zeki et al., 1991; Tootell et al., 1995; Seiffert et al., 2003; Smith et al., 2006). Runs used for the functional localizer were excluded from further analyses. We used a general linear model (GLM) to contrast BOLD responses acquired during motion conditions (0%, 30%, and 100%) with twinkle and rest conditions. Voxels that responded more strongly to moving stimuli at the ascending tip of the inferior temporal sulcus and in or around the calcarine sulcus were identified as hMT+ (minimum number of voxels = 117, M = 226, SD = 31) and V1 (minimum number of voxels = 53, M = 481, SD = 106), respectively. No significant difference in the BOLD responses was observed between the right and left hemispheres ($F(1,18) = 0.073$, $p = 0.79$). Thus, further analyses were conducted using data averaged across hemispheres. Statistical analyses were performed on BOLD responses based on beta weight values calculated with the GLM within the two ROIs. Each motion coherence condition was contrasted with twinkle and rest conditions. To compare the BOLD responses at the group level, a 2 × 2 × 3 mixed-design ANOVA was conducted with group (CVI and controls), brain area (V1 and hMT+), and motion coherence level (0%, 30%, and 100%) as factors. To investigate the effect of motion coherence level for the control and CVI groups in V1 and hMT+ independently, we conducted two 2 × 3 mixed-design ANOVAs with group and motion coherence as factors.

2.3.2. HARDI data processing and analysis

Pre-processing of the HARDI data was performed in accordance to previous publications by our group (e.g. Bauer et al., 2014b; Bauer et al., 2017a; Bauer and Papadelis, 2019). Briefly, each participant's data was skull stripped and corrected for eddy-currents and subject movement (FSL 6.0.3 - FMRIB Software Library, http://fsl.fMRib.ox.ac.uk/fsl) (Andersson et al., 2016; Andersson and Sotiropoulos, 2016). The orientation distribution function (ODF) was reconstructed in DSI-Studio (http://dsi-studio.labsolver.org) using generalized q-sampling imaging (GQI) (Yeh et al., 2010) and according to the following parameters: diffusion sampling length ratio = 1.25, ODF sharpening via decomposition (Yeh and Tseng, 2013), decomposition fraction = 0.04, maximum fiber population = 8, fibers resolved per voxel = 3, ODF tessellation = 8-fold. Each of the functionally defined ROIs (V1 and hMT+) and the anatomically-defined thalamic nuclei [lateral geniculate nucleus (LGN), as well as the lateral, medial, and inferior pulvinar (PUL, PUM, and PUI, respectively)] (Keller et al., 2012; Iglesias et al., 2018) were reverse transformed into subject-specific HARDI space, creating the seed (start) and target (end) point ROIs for tractography analysis. DSI-Studio generated streamlines between the ROIs with the following user-defined parameters: termination angle of 90°, subject-specific quantitative anisotropy (QA) threshold (range 0.05 to 0.17, mean 0.08, sd 0.0345) (Bauer et al., 2017b), smoothing of 1, step size 0 mm, minimum length = 5 mm, maximum length = 300 mm, subvoxel seed position, random seed orientation, trilinear interpolation, and 100,000 seeds. For each tract, a bidirectional seeding approach was used. Structural outcomes of interest were tract volume, quantitative anisotropy (QA), along with mean (MD), axial (AD), and radial (RD) diffusivities. Group differences in outcome variables were determined using Mann-Whitney *U* test followed by a correction for multiple comparisons using FDR ($p < 0.05$).

2.4. Correlation analysis

We investigated potential associations of interest between motion coherence thresholds with functional and white matter connectivity outcomes using Spearman's rank sum correlations and adjusting for multiple comparisons using an FDR correction. As this was an exploratory analysis, we applied an FDR threshold of 0.1.

3. Results

3.1. Behavioral results

Mean motion coherence threshold for CVI participants (44.18% ± 23.3 SD) was significantly higher (i.e. indicative of worse performance) compared to controls (15.49% ± 8.01 SD) ($U = 18$, $Z = 3.6407$, $p < 0.0001$) (Fig. 1). Inspecting the distribution of individual threshold values also revealed greater response variability within the CVI group compared to controls.

With respect to associated causes of CVI, it was noted that mean coherence threshold was higher for CVI associated with PVL (52.36% ± 19.9 SD) compared to non-PVL (37.36% ± 25.4 SD). However, this difference was not statistically significant ($p = 0.41$). In the CVI group, there was also no significant correlation between age and motion coherence threshold (rho = 0.44, p = 0.17), as well as between visual acuity and motion coherence threshold (rho = 0.08, p = 0.79).

3.2. fMRI analysis

The main fMRI analysis focused on comparing BOLD responses (reported as beta weight values) within areas V1 and hMT+ and across different motion coherence levels (i.e. 0%, 30%, and 100%) contrasted with the twinkle and rest conditions (Fig. 2). Overall, there was a significant main effect of ROI ($F(1,18) = 19.65$, $p = 0.0003$) and motion coherence level ($F(2,36) = 7.14$, $p = 0.009$), with significant interactions

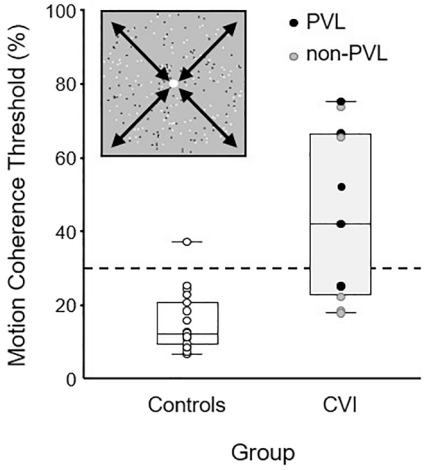

Fig. 1. Individual (circles) and mean (shown as box plot presenting the ranges from the first quartile to the third quartile of the distribution and the line across the bar and whiskers indicate the median and the most extreme data points, respectively) motion coherence thresholds for CVI and control participants in response to the RDK optic flow stimulus (shown in inset figure). Compared to controls, CVI participants required a higher coherence signal in order to correctly identify the direction of motion (expansion or contraction) of the optic flow stimulus. Dashed line corresponds to 30% coherence level used in the subsequent fMRI experiment, which was below the mean threshold for CVI group and above that of controls. Note similar distribution in performance for CVI participants associated with PVL and non-PVL causes.

between coherence level and group ($F(2,36) = 5.86$, $p = 0.01$), and between ROI and coherence level ($F(2,36) = 12.25$, $p = 0.0003$). There was no overall effect of group ($F(1,18) = 3.16$, $p = 0.09$). Further details regarding the time course responses are provided in the supplemental Fig. 2 A.

To further investigate the interaction between group and coherence level in V1 and hMT+, we applied 2 (group) × 3 (coherence level) factor mixed-design ANOVAs. In V1, there was a significant main effect of coherence level ($F(2,36) = 12.09$, $p < 0.0001$) whereby BOLD responses decreased with increasing motion coherence levels. The effect of group was not significant ($F(1,18) = 1.33$, $p = 0.26$), nor was the interaction between group and coherence level ($F(2,36) = 1.91$, $p = 0.16$). In area hMT+, there was no significant main effect of coherence ($F(2,36) = 1.47$, $p = 24$). However, there was a significant group effect ($F(1,18) = 5.42$, $p = 0.03$) whereby BOLD responses were lower in CVI (M = 1.09, SEM = 0.14) compared to controls (M = 1.63, SEM = 0.18). Furthermore, there was a significant interaction between coherence and group ($F(2,36) = 8.64$, $p = 0.001$). Specifically, increased motion coherence was associated with an increased BOLD signal response in area hMT+ for CVI, but not for the control group.

A series of paired-sample t-tests (FDR-corrected) were then applied to evaluate the effect of motion coherence levels on BOLD signal responses in areas V1 and hMT+ in each group separately. In area V1, there was a significant reduction in BOLD response at 100% compared to 0% coherence in the control group ($t(10) = 4.57$, FDR $p = 0.006$). No other comparisons reached statistical significance in area V1. In area hMT+, we observed a differential response in CVI compared to controls in that there was a significant increase in BOLD response at 100% coherence compared to 0% coherence in the CVI group ($t(8) = 3.72$, FDR $p = 0.012$), while decreased responses were observed in the control group ($t(10) = 1.96$, FDR $p = 0.09$). Finally, a significant reduction in BOLD response was observed for the CVI group compared to controls at both 0% ($t(18) = 3.38$, FDR $p = 0.012$) and 30% coherence ($t(18) = 2.51$, FDR $p = 0.033$).

To characterize possible effects related to surround suppression responses related to our visual stimulus, we computed a coherence index (CI) defined as CI = $BOLD_H$-$BOLD_L$ [where $BOLD_H$ and $BOLD_L$ stand for BOLD responses evoked by high (100%) and low (0% or 30%) coherence, respectively]. A positive CI is consistent with increased BOLD responses with increased coherence (i.e. facilitation) while a negative CI suggests decreased BOLD responses with increased coherence (i.e. suppression). In area V1, a negative CI was observed for both groups, consistent with an overall suppression effect. In area hMT+, a negative CI was revealed for the control group (i.e. suppression), while a positive CI was shown for the CVI group, consistent with an overall facilitation effect (Fig. 3). To see whether CI values were significantly different than null (i.e. 0), we applied one-sample two-tailed Student's t-tests. In V1, CI was significantly less than zero (i.e. suppression) for controls for the 100%-0% condition ($t(10) = 4.57$, FDR $p = 0.008$ and 100%-30% condition ($t(10) = 3.18$, FDR $p = 0.026$) whereas CI was significantly greater than zero (i.e. facilitation) for the 100%-0% condition in hMT+ for CVI ($t(8) = 3.72$, FDR $p = 0.024$). Further details regarding the time course responses are provided in the supplemental Fig. 2 B.

3.3. White matter tract reconstruction and analysis

Direct white matter tracts between the functionally-defined ROI areas V1 and hMT+ were successfully reconstructed in at least one hemisphere for all participants, with bilateral tract reconstruction possible in all controls and in half (4 out of 8) of the CVI participants (right hemisphere tracts only in the remaining 4 CVI participants). Tracts between thalamic nuclei and area hMT+ were successfully reconstructed bilaterally in 6 participants (2 out of 8 controls, and 4 out

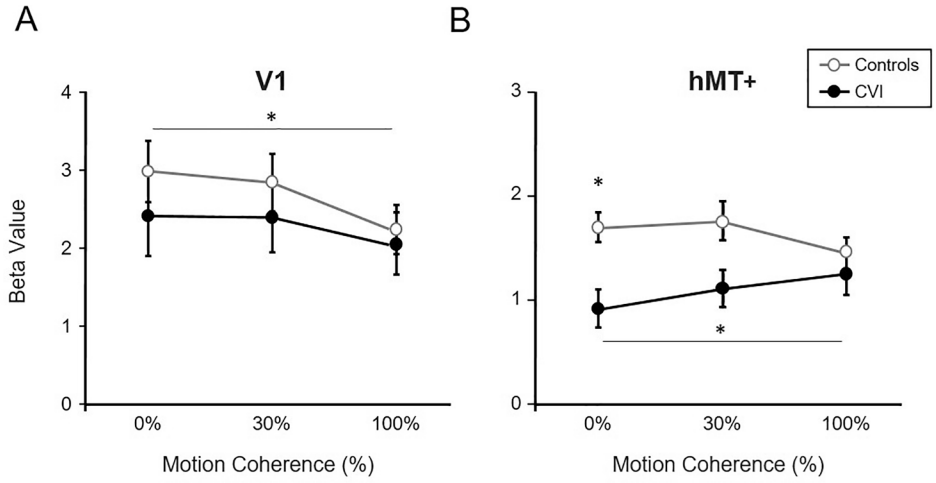

Fig. 2. BOLD signal responses (expressed as beta weights) in areas V1 (A) and hMT+ (B). In V1, BOLD activation was not statistically different between CVI and controls with respect to increasing motion coherence levels. In both groups, there was an overall trend of reduced activation with increased motion coherence levels in V1. In area hMT+, BOLD activation was reduced overall in CVI compared to controls. Furthermore, responses increased with increasing motion coherence in CVI, while in controls responses remained unmodulated. Error bars represent ± SEM. *$p < 0.05$.

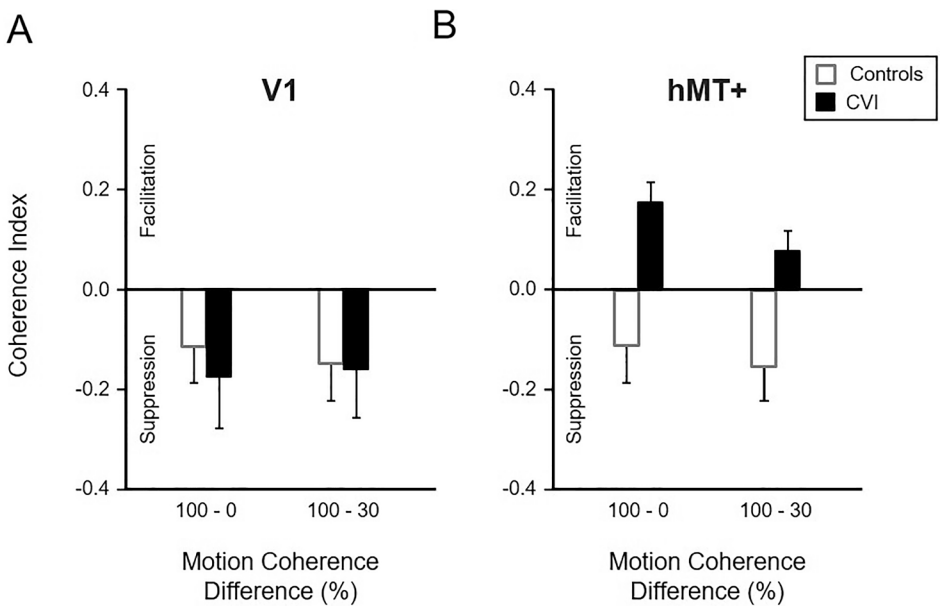

Fig. 3. Mean Coherence Indices (CI) computed using beta weight values. A negative and positive CI value are indicative of a surround suppression and facilitation effect, respectively. In V1, comparing responses from 100% to 0% and 100%-30% coherence show suppression in both control and CVI groups (A). However, in hMT+, controls show overall suppression whereas CVI participants show a facilitation effect which may be an indicative of an impaired surround suppression mechanism (B). Error bars represent SEM.

of 8 participants with CVI) and only in one hemisphere in 6 out of 16 participants (3 controls in right only, 1 control and 2 CVI in left only). No thalamo-hMT+ tracts were identified in 2 controls and 2 participants with CVI. Representative white matter tract reconstructions are shown in Fig. 4. No significant differences in QA or volume of the thalamo-hMT+ tracts were observed following correction for multiple comparisons. Although bilateral increases in MD and

RD were observed for the V1-hMT+ tract, only outcomes in the right hemisphere survived FDR correction (median MD CVI = 0.28 ± 0.04 SD, median MD control = 0.21 ± 0.02 SD, Z = 2.9406, FDR p = 0.0308; median RD CVI = 0.20 ± 0.03 SD, median RD control = 0.13 ± 0.02 SD, Z = 3.3607, FDR p = 0.0112). AD values were also greater for the V1-hMT+ tract and survived FDR correction in the left hemisphere (median AD CVI = 0.45 ± 0.07 SD, median AD control = 0.35 ± 0.05 SD, Z = 2.3778, FDR p = 0.0487). No group differences in tractography outcomes for thalamo-hMT+ tracts survived FDR correction. Complete results and details are provided in Table 2.

3.4. Correlation analysis

As an exploratory analysis, we investigated potential associations between motion coherence thresholds and outcomes from our functional and diffusion based imaging data. After FDR correction, we observed a negative correlation within area V1 at 0% and 30% coherence levels (n = 18, rho_{30} = -0.57, p_{30} = 0.0126, FDR p_{30} = 0.0794; rho_0 = -0.56, p_0 = 0.0147, FDR p_0 = 0.0794) suggesting a potential association between lower beta values and higher motion coherence thresholds (i.e. lower responses were associated with poorer performance on the optic flow task). Motion coherence threshold was also found to be correlated with white matter volume (n = 15, rho = -0.63, p = 0.0121, FDR p = 0.0794) and RD (n = 15, rho = 0.69, p = 0.0045, FDR p = 0.0794) within the right V1-hMT+ tract, along with AD of the left thalamo-hMT+ tract (n = 9, rho = 0.82, p = 0.0072, FDR p = 0.0794). Specifically, smaller tracts and increased axial and radial diffusivities were associated with poorer performance on the optic flow task.

4. Discussion

In this study, we used a combined behavioral and multi-modal imaging approach to investigate the neurophysiological basis of global motion processing deficits in CVI. We found that mean motion coherence threshold in response to viewing a RDK optic flow task was significantly higher in CVI participants compared to controls. On average, individuals with CVI required nearly three times the motion coherence signal in order to reliably detect the direction of movement of the optic flow stimulus. Using fMRI, we observed similar BOLD signal response profiles between the CVI and control groups in area V1, while notable differences were observed in area hMT+. In particular, BOLD responses in hMT+ were significantly weaker in the CVI group at lower levels of motion coherence. In controls, BOLD responses remained relatively unchanged with increased motion coherence levels while in the CVI group, responses increased with increasing motion coherence levels. This discrepancy in response profile is likely an indication of impaired intrinsic surround modulation mechanisms in CVI, which typically characterize responses in area hMT+. Furthermore, white matter tract reconstruction revealed that CVI was associated with a greater impact on the integrity of cortico-cortical compared to thalamo-cortical connections. Specifically, we observed significant increases in all diffusivity indices (i.e. mean, radial, and axial) within V1-hMT+ connections. In contrast, group comparisons with respect to thalamo-hMT+ tracts showed no differences with respect to the diffusion outcomes analyzed. Finally, a number of functional neuroimaging and white matter structural outcomes were associated with behavioral performance. At the level of hMT+, smaller tract volume and alterations in diffusivity consistent with aberrant myelination (e.g. increased radial diffusivity) (Song, Sun et al., 2002; Jones, Knosche et al., 2013; Ajina et al., 2015b) were correlated with increased motion coherence thresholds (i.e. poorer performance).

Our behavioral finding of elevated motion coherence thresholds in CVI is consistent with previous reports of global motion and visuospatial processing deficits in this population. Similar outcomes have also been observed in populations at risk for CVI, including individuals with cerebral palsy (CP) and children born with extremely low birth weight (Pavlova et al., 2003; MacKay et al., 2005; Guzzetta et al., 2009; Taylor et al., 2009; Weinstein et al., 2012; Bhat et al., 2021) and growing evidence suggests that impaired visual motion processing appears to be a common consequence of premature birth and early neurological injury (see (Braddick et al., 2003; Johnston et al., 2017) for reviews). Also consistent with previous studies, we noted that inter-individual behavioral responses were highly variable within the CVI group (e.g. (Weinstein et al., 2012; Bhat et al., 2021)). Moreover, impairments in motion coherence threshold in CVI participants were not correlated with visual acuity, and elevated motion coherence thresholds were also found in individuals with normal (or near normal) visual acuity. Taken together,

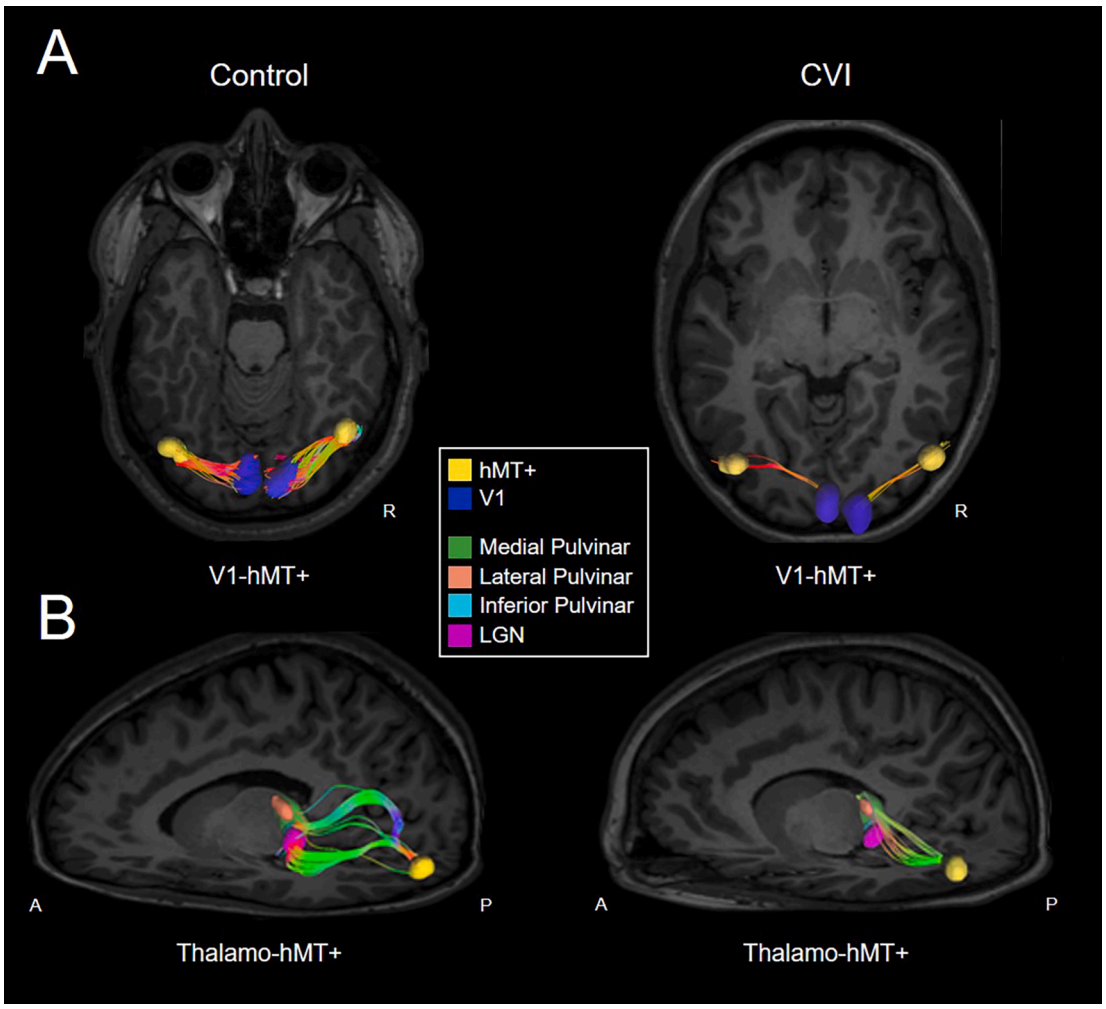

Fig. 4. Reconstruction of white matter tracts in a representative control and CVI participant (left and right panel, respectively). (A) Bilateral connections between areas V1-hMT+ (axial plane) and (B) thalamo-hMT+ (sagittal plane, left hemisphere) are shown. For V1-hMT+ connections, note that the fiber tracts follow a similar trajectory in both the control and CVI participants. Overall, group structural changes between CVI and controls were more evident at the level of cortico-cortical (V1-hMT+) than thalamo-hMT+ connections. Statistically significant differences were observed with respect to diffusivity measures in CVI compared to controls, which were suggestive of aberrant myelination and axonal injury. Colored legend correspond to the location of functionally and anatomically defined ROIs used for the purposes of tract reconstruction.

this suggests that observed group differences in our study are likely related to changes in underlying neurophysiology rather than simply impaired visual acuity. Furthermore, this finding highlights the value of using novel psychophysical approaches (such as moving RDK patterns) to help uncover higher order visual processing deficits which could be potentially overlooked, particularly in cases where visual acuity function is within normal range (van Genderen et al., 2012).

Previous research has attempted to identify the neurophysiological basis of motion perception deficits observed in children with neurodevelopmental disorders associated with CVI. However, there appears to be conflicting evidence regarding the locus of these visual deficits, with some studies suggesting abnormal processing occurring as early as V1, while others propose an impairment of signal integration at the level of area hMT+. Regarding the former view, a recent study found that cortical thickness (but not grey matter volume) changes within area V1 were negatively correlated with motion coherence sensitivity (assessed using a rotating RDK visual pattern) in children with visual processing deficits related to PVL (Bhat et al., 2021). However, this association was not found within higher order visual processing areas including areas MT, MST, and the IPS (Bhat et al., 2021). Despite differences with respect to the methodological approaches employed, the results from our current study do not appear to align with these findings but, are not completely contradictory. Specifically, at early visual processing stages (i.e. V1), we found that response profiles were similar across increasing motion coherence levels in both CVI and control participants, suggestive of intact processing of local motion signals. In contrast, responses in area hMT+ of CVI participants were comparatively lower than that of controls (particularly at lower coherence levels), indicating that global motion processing deficits may be related to aberrant responses within this higher order visual area. Previous electrophysiological studies also support this view. One study analyzed steady state visual evoked potentials (ssVEP) in CVI associated with PVL and in response to viewing local and global motion stimuli (rotating RDK patterns) (Weinstein et al., 2012). Comparing occipital activation responses (i.e. signal amplitudes) with individuals with ocular visual impairment (i.e. amblyopia and/or strabismus) and neurotypical controls, it was found that CVI participants showed selective global (but not local) motion processing deficits, especially for slower stimulus velocities (Weinstein et al., 2012). More recently, activity within area MT/V5 was examined using magnetoencephalography (MEG) in children with visual processing deficits associated with CP (VerMaas et al., 2019). Viewing a horizontal moving grating stimulus in both CP and control participants resulted in changes in the strength of oscillations in area MT/V5 and within the theta-alpha (5–10 Hz) and alpha–beta (8–20 Hz) bands. However, these alpha–beta

Table 2
White Matter Tractography Results.

Variable		Group	Median	Std Dev	Z	FDR, *p < 0.05
Left V1-hMT+						
	Volume	CVI	−681.45	252.82	−0.85	0.50
		Control	−60.02	1468.63		
	QA	CVI	0.15	0.01	1.70	0.13
		Control	0.12	0.02		
	MD	CVI	0.28	0.05	2.04	0.08
		Control	0.20	0.03		
	AD	CVI	0.45	0.07	2.38	0.0487*
		Control	0.35	0.05		
	RD	CVI	0.19	0.05	1.70	0.19
		Control	0.12	0.02		
Right V1-hMT+						
	Volume	CVI	−269.66	290.06	−1.89	0.15
		Control	324.77	658.87		
	QA	CVI	0.13	0.07	−0.42	0.73
		Control	0.14	0.04		
	MD	CVI	0.28	0.04	2.94	0.0308*
		Control	0.21	0.02		
	AD	CVI	0.44	0.07	1.47	0.28
		Control	0.37	0.04		
	RD	CVI	0.20	0.03	3.36	0.0112*
		Control	0.13	0.02		
Left Thalamus-hMT+						
	Volume	CVI	−625.59	1259.44	1.29	0.31
		Control	−3.90	1751.98		
	QA	CVI	0.14	0.07	1.03	0.42
		Control	0.22	0.05		
	MD	CVI	0.27	0.04	−2.32	0.08
		Control	0.20	0.03		
	AD	CVI	0.47	0.05	−1.81	0.17
		Control	0.39	0.04		
	RD	CVI	0.17	0.04	−2.07	0.12
		Control	0.10	0.03		
Right Thalamus-hMT+						
	Volume	CVI	342.87	699.36	0.98	0.44
		Control	−501.08	920.70		
	QA	CVI	0.18	0.05	1.22	0.33
		Control	0.17	0.02		
	MD	CVI	0.26	0.07	−0.24	0.81
		Control	0.31	0.06		
	AD	CVI	0.45	0.08	−0.73	0.55
		Control	0.47	0.07		
	RD	CVI	0.16	0.06	−0.24	0.81
		Control	0.23	0.05		

oscillations were weaker in children with CP and further, were correlated with slower response times and less accuracy in identifying a change in the direction of the moving stimulus (VerMaas et al., 2019). Evidence from these latter electrophysiological studies highlight the importance of area hMT+ and are consistent with associating motion processing deficits within this higher order visual processing stage.

While there is mounting evidence implicating the role of area hMT+ with impaired global motion processing in CVI, questions still remain as to the exact underlying mechanisms and their relationship to the clinical profile of this population. Along with decreased levels of BOLD signal activation, our data suggest that impaired surround suppression mechanisms may also be a contributing factor. It is known that a neuron's response can be modulated by a surround stimulus when its classical receptive field (cRF) and surround are stimulated together (Angelucci et al., 2017). Furthermore, surround influences can vary with context. When cRF drive is weak, surround stimuli that match properties of the cRF stimuli can facilitate responses, but when cRF drive is robust, the same surround stimuli can have a suppressive influence (Toth et al., 1996; Somers et al., 1998). Facilitative and/or suppressive surround influences in area hMT+ have been well described (see (Previc et al., 2000; Ajina et al., 2015a)) and characterized using fMRI (Zenger-Landolt and Heeger, 2003; Turkozer et al., 2016; Schallmo et al., 2018; Er et al., 2020). In this experiment, our visual stimulus was sufficiently large (21.3° in diameter) to stimulate both the center and surround areas of a typical hMT+ receptive field (Albright and Desimone, 1987). Furthermore, our computed coherence index (CI) data confirm that responses in area hMT+ in controls were consistent with surround suppression (i.e. a negative coherence index); while in CVI, we observed a relative facilitation response (i.e. a positive coherence index) suggestive of a weaker surround suppression mechanism. Motion selectivity in area hMT+ is believed to emerge shortly after birth however, the perceptual correlates of center-surround modulation mechanisms are first seen around 7 to 8 months (Nakashima et al., 2019). This suggests that these suppressive mechanisms develop after early sensitivity to motion signals. In the setting of CVI, it is possible that perinatal injury may impact the development of critical integration and segregation processing mechanisms within hMT+ (Tadin, 2015). Interestingly, this profile of impaired intrinsic surround suppression responses has also been reported in other clinical populations with neurodevelopmental and psychiatric conditions such as autism (Schallmo et al., 2020) and schizophrenia (Tadin et al., 2006). Therefore, we speculate that impaired surround suppression mechanisms in area hMT+ may also play a contributory role in the impaired global perception of optic flow patterns we observed in CVI.

Underlying changes in white matter cortico-cortical connectivity are also likely to contribute to our observations of global motion processing impairments in CVI. Results from our white matter tract reconstruction and analyses suggest that the aberrant response profile observed in area hMT+ may also be related to changes in radial diffusivity (which is suggestive of reduced myelination (Song et al., 2002; Jones et al., 2013; Ajina et al., 2015b) between key cortico-cortical areas. Specifically, we found a greater impact on V1-hMT+ compared to thalamo-hMT+ connectivity in CVI with significant increases in axial diffusivity (AD) in left V1-hMT+ connections, and increased mean diffusivity (MD) and radial diffusivity (RD) in right V1-hMT+ connections in CVI compared to controls. A strong negative correlation between white matter volume and positive correlation between RD of right V1-hMT+ and motion coherence thresholds were also observed. Diffusion outcomes such as anisotropy and diffusivity are sensitive to various underlying changes in tissue properties and, as such, are common indices of tissue microstructure and potential neuronal damage (Jones, 2008; Jones et al., 2013). Increased RD may reflect underlying aberrant myelination, while changes in AD may represent axonal injury, and increased MD is generally associated with white matter damage (Song et al., 2002; Jones et al., 2013; Ajina et al., 2015a). However, caution should be taken in interpreting diffusivity outcomes as they can reflect a number of underlying tissue properties which in turn, make precise determinations regarding physiological mechanisms challenging (see Takahashi et al., 2002 and Jones et al., 2013 for further discussion). In the case of CVI, neurohistological studies indicate that many etiologies of CVI (including PVL) are associated with aberrant patterns of myelination due to damage to developing oligodendrocytes (Volpe, 2009). As such, we feel relatively confident that the increased RD observed in our CVI participants likely reflects aberrant myelination. Indeed, the detection of moving stimuli requires the integration of signals from disparate brain regions with precise temporal dynamics. Because myelin enables the rapid transmission of action potentials, it is critical for normal motion processing (Biagi et al., 2015). Accordingly, we may anticipate impairments in the processing of moving stimuli along pathways where myelin is reduced. Along these lines, it is not surprising that we observed a positive correlation between RD and motion coherence thresholds, whereby higher levels of RD (i.e. aberrant myelination) in right V1-hMT+ tracts were associated with higher motion coherence thresholds (i.e. poorer global motion processing abilities). This is in agreement with previous studies reporting associations between various visual impairments and aberrant white matter development in CVI (Guzzetta et al.,

2010; Ortibus et al., 2012; Guzzetta et al., 2013; Lennartsson et al., 2014).

While the current study focused on the relative contribution of areas V1 and hMT+, it is important to recognize that impaired global motion processing in CVI may well implicate other regions. It is well established that the analysis of complex moving scenes involves a network of brain regions including V3A, V6, and the intraparietal sulcus (IPS) (Tootell et al., 1997; Braddick et al., 2000; Pitzalis et al., 2006; Putcha et al., 2014). In addition, frontal cortical areas (e.g. areas 8 and 46 in the macaque; corresponding to human posterior middle frontal gyrus and dorsolateral prefrontal cortex, respectively; (Sallet et al., 2013; Neubert et al., 2014) have been suggested to provide top-down control of motion perception (Kim and Shadlen 1999), while medial prefrontal cortex appears to be implicated in spatial working memory components of self-navigation (Sherrill et al., 2015). Interestingly, Atkinson (2017) proposed that individual motion processing abilities are more likely related to decision making and attention control mechanisms rather than integration at the level of higher order visual processing areas (Atkinson, 2017). Finally, at the subcortical level, direct connections (via the pulvinar and lateral geniculate nucleus; (Sincich et al., 2004; Schmidt et al., 2010) have also been identified, and may have increased relevance with regard to residual motion processing abilities in the setting of striate cortical damage (Ajina et al., 2015b).

Taken together, our behavioral results, evidence of an aberrant response profile within area hMT+ (including impaired activation and suppression responses), and evidence of impaired white matter structural connectivity between areas V1-hMT+ appear to support the view of CVI within the context of "dorsal stream dysfunction" (Dutton, 2009; Macintyre-Béon et al., 2013; Dutton et al., 2017). Along with visuospatial and complex motion processing, other associated dorsal stream functions include the analysis of visual scene complexity, selectively deploying visual attention, and the suppressing of distractor elements (Dutton et al., 2006). Given that area hMT+ is a key region along the dorsal visual stream, we can begin to develop a neurophysiological basis to explain visuospatial and motion processing deficits reported in CVI. A potential explanation for the observed impaired responses in hMT+ may be related to the maldevelopment of the underlying white matter fasciculi. More specifically, aberrant responses and cortico-cortical connections are likely to implicate various branches of the superior longitudinal fasciculus (SLF) which corresponds to the neuroanatomical correlate of the dorsal visual processing stream (Thiebaut de Schotten et al., 2011). Along these lines, Braddick and coworkers (2017) found that in neurotypical developed children, global motion sensitivity was correlated with SLF integrity (Braddick et al., 2017). Further, Braddick and colleagues further proposed that motion sensitivity may be more reliant on these fronto-parietal networks than subcortical or early visual areas (Braddick et al., 2017). Finally, preliminary work by our group demonstrated that CVI is associated with a marked reduction in the volume of the SLF compared to controls with neurotypical development (Bauer et al. 2014a; Bauer and Papadelis, 2019). Future investigations parsing the SLF into its anatomical divisions will be necessary to more precisely determine the structural correlates of these changes in association with visuospatial processing deficits.

Finally, it is important to recognize a number of limitations with this study. First, despite the advantages of associating behavioral findings with both functional and structural imaging data, conclusions should be interpreted with caution given the relatively small sample size. Challenges with demands related to carrying out both the behavioral and imaging components place limitations not only in terms of recruiting appropriate participants, but also may lead to a potential selection bias (see also Bhat et al., 2021). Furthermore, fMRI responses were investigated at only three coherence levels. Incorporating a parametric design with a wider range of coherence levels, stimulus sizes, as well as measurement of detection duration thresholds, may help better characterize response profiles and associated patterns of activation. At the same time, a systematic investigation of center-surround modulation profiles using well-studied perceptual correlates of surround suppression (i.e. spatial suppression; see Tadin et al., 2003) is also warranted. While a fixation task was employed to ensure optimal task attentiveness, continuous eye movement tracking could help reveal potential group differences with respect to fixation abilities and what aspects of the visual stimulus are being viewed to determine the global direction of motion. Lastly, future studies should investigate response profiles within a larger network of cortical and subcortical areas implicated with complex motion processing in relation to the severity of CVI.

5. Conclusion

This study aimed to investigate the neural correlates associated with impaired global motion processing in individuals with CVI. Behaviorally, we found that mean motion coherence threshold related to the perception of RDK optic flow patterns was significantly higher in CVI compared to controls with neurotypical development. We also observed reduced BOLD signal activation and a response profile consistent with impaired surround suppression in area hMT+, as well as structural changes within white matter tracts connecting V1 to hMT+. The results of this study suggest that deficits in global motion processing observed in CVI are consistent with dorsal stream dysfunction, and may be explained by a combination of impaired integration and segregation mechanisms as well as white matter integrity at the level of area hMT+.

Author contribution

All authors contributed to the design, analysis of results, and preparation of this manuscript. All named authors meet the International Committee of Medical Journal Editors (ICMJE) criteria for authorship for this article. The authors take responsibility for the integrity of the work as a whole, and have given their approval for this version to be published.

Declaration of Competing Interest

The authors declare that they have no known competing financial interests or personal relationships that could have appeared to influence the work reported in this paper.

Appendix A. Supplementary data

Supplementary data to this article can be found online at https://doi.org/10.1016/j.nicl.2021.102821.

References

Ajina, S., Kennard, C., Rees, G., Bridge, H., 2015a. Motion area V5/MT+ response to global motion in the absence of V1 resembles early visual cortex. Brain 138 (1), 164–178.
Ajina, S., Pestilli, F., Rokem, A., Kennard, C., Bridge, H., 2015b. Human blindsight is mediated by an intact geniculo-extrastriate pathway. elife 4, e08935.
Albright, T.D., Desimone, R., 1987. Local precision of visuotopic organization in the middle temporal area (MT) of the macaque. Exp. Brain Res. 65 (3), 582–592.
Anderson, V., Spencer-Smith, M., Wood, A., 2011. Do children really recover better? Neurobehavioural plasticity after early brain insult. Brain 134 (8), 2197–2221.
Andersson, J.L.R., Graham, M.S., Zsoldos, E., Sotiropoulos, S.N., 2016. Incorporating outlier detection and replacement into a non-parametric framework for movement and distortion correction of diffusion MR images. Neuroimage 141, 556–572.
Andersson, J.L.R., Sotiropoulos, S.N., 2016. An integrated approach to correction for off-resonance effects and subject movement in diffusion MR imaging. Neuroimage 125, 1063–1078.
Angelucci, A., Bijanzadeh, M., Nurminen, L., Federer, F., Merlin, S., Bressloff, P.C., 2017. Circuits and mechanisms for surround modulation in visual cortex. Annu. Rev. Neurosci. 40, 425–451.
Atkinson, J., 2017. The Davida Teller Award Lecture, 2016: Visual Brain Development: A review of "Dorsal Stream Vulnerability"-motion, mathematics, amblyopia, actions, and attention. J. Vis. 17 (3), 26.
Bauer, C.M., G. Heidary, B. B. Koo, R. Killiany and L. B. Merabet (2014). Extrageniculostriate visual pathway changes in cortical visual impairment characterized by HARDI. Organization for Human Brain Mapping (OHBM Abstracts).

Bauer, C.M., Hirsch, G.V., Zajac, L., Koo, B.B., Collignon, O., Merabet, L.B., 2017a. Multimodal MR-imaging reveals large-scale structural and functional connectivity changes in profound early blindness. PLoS ONE 12 (3), e0173064.
Bauer, C.M., Papadelis, C., 2019. Alterations in the structural and functional connectivity of the visuomotor network of children with periventricular leukomalacia. Semin. Pediatr. Neurol. 31, 48–56.
Bauer, C.M., Heidary, G., Koo, B.-B., Killiany, R.J., Bex, P., Merabet, L.B., 2014b. Abnormal white matter tractography of visual pathways detected by high-angular-resolution diffusion imaging (HARDI) corresponds to visual dysfunction in cortical/cerebral visual impairment. J. AAPOS 18 (4), 398–401.
Bauer, C.M., Zajac, L.E., Koo, B.B., Killiany, R.J., Merabet, L.B., 2017b. Age-related changes in structural connectivity are improved using subject-specific thresholding. J. Neurosci. Methods 288, 45–56.
Bhat, A., Biagi, L., Cioni, G., Tinelli, F., Morrone, M.C., 2021. Cortical thickness of primary visual cortex correlates with motion deficits in periventricular leukomalacia. Neuropsychologia 151, 107717.
Biagi, L., Crespi, S.A., Tosetti, M., Morrone, M.C., 2015. BOLD response selective to flow-motion in very young infants. PLoS Biol. 13 (9), e1002260.
Boot, F.H., Pel, J.J.M., van der Steen, J., Evenhuis, H.M., 2010. Cerebral Visual Impairment: which perceptive visual dysfunctions can be expected in children with brain damage? A systematic review. Res. Dev. Disabil. 31 (6), 1149–1159.
Braddick, O., Atkinson, J., Wattam-Bell, J., 2003. Normal and anomalous development of visual motion processing: motion coherence and 'dorsal-stream vulnerability'. Neuropsychologia 41 (13), 1769–1784.
Braddick, O., Atkinson, J., Akshoomoff, N., Newman, E., Curley, L.B., Gonzalez, M.R., Brown, T., Dale, A., Jernigan, T., 2017. Individual differences in children's global motion sensitivity correlate with TBSS-based measures of the superior longitudinal fasciculus. Vision Res. 141, 145–156.
Braddick, O.J., O'Brien, J.M.D., Wattam-Bell, J., Atkinson, J., Turner, R., 2000. Form and motion coherence activate independent, but not dorsal/ventral segregated, networks in the human brain. Curr. Biol. 10 (12), 731–734.
Braddick, O.J., O'Brien, J.M.D., Wattam-Bell, J., Atkinson, J., Hartley, T., Turner, R., 2001. Brain areas sensitive to coherent visual motion. Perception 30 (1), 61–72.
Buracas, G.T., Albright, T.D., 1996. Contribution of area MT to perception of three-dimensional shape: a computational study. Vision Res. 36 (6), 869–887.
Cui, Y., Liu, L.D., Khawaja, F.A., Pack, C.C., Butts, D.A., 2013. Diverse suppressive influences in area MT and selectivity to complex motion features. J. Neurosci. 33 (42), 16715–16728.
Durant, S., Zanker, J.M., 2012. Variation in the local motion statistics of real-life optic flow scenes. Neural Comput. 24 (7), 1781–1805.
Dutton, G.N., 2009. 'Dorsal stream dysfunction' and 'dorsal stream dysfunction plus': a potential classification for perceptual visual impairment in the context of cerebral visual impairment? Dev. Med. Child Neurol. 51 (3), 170–172.
Dutton, G.N., 2013. The spectrum of cerebral visual impairment as a sequel to premature birth: an overview. Doc. Ophthalmol. 127 (1), 69–78.
Dutton, G. N. and A. H. Lueck (2015). Impairment of vision due to damage to the brain. Vision and the brain: Understanding cerebral visual impairment in children. A. H. Lueck and G. N. Dutton. New York, NY, AFB Press: 3-20.
Dutton, G.N., McKillop, E.C., Saidkasimova, S., 2006. Visual problems as a result of brain damage in children. Br. J. Ophthalmol. 90 (8), 932–933.
Dutton, G.N., Chokron, S., Little, S., McDowell, N., 2017. Posterior parietal visual dysfunction: An exploratory review. Vision Dev. Rehab. 3 (1), 10–22.
Er, G., Pamir, Z., Boyaci, H., 2020. Distinct patterns of surround modulation in V1 and hMT. Neuroimage 220, 117084.
Fazzi, E., Signorini, S.G., Bova, S.M., La Piana, R., Ondei, P., Bertone, C., Misefari, W., Bianchi, P.E., 2007. Spectrum of visual disorders in children with cerebral visual impairment. J. Child Neurol. 22 (3), 294–301.
Fiori, S., Cioni, G., Klingels, K., Ortibus, E., Van Gestel, L., Rose, S., Boyd, R.N., Feys, H., Guzzetta, A., 2014. Reliability of a novel, semi-quantitative scale for classification of structural brain magnetic resonance imaging in children with cerebral palsy. Dev. Med. Child Neurol. 56 (9), 839–845.
Guzzetta, A., Tinelli, F., Del Viva, M.M., Bancale, A., Arrighi, R., Pascale, R.R., Cioni, G., 2009. Motion perception in preterm children: role of prematurity and brain damage. NeuroReport 20 (15), 1339–1343.
Guzzetta, A., D'Acunto, G., Rose, S., Tinelli, F., Boyd, R., Cioni, G., 2010. Plasticity of the visual system after early brain damage. Dev. Med. Child Neurol. 52 (10), 891–900.
Guzzetta, A., Fiori, S., Scelfo, D., Conti, E., Bancale, A., 2013. Reorganization of visual fields after periventricular haemorrhagic infarction: potentials and limitations. Dev. Med. Child Neurol. 55 (Suppl 4), 23–26.
Iglesias, J.E., Insausti, R., Lerma-Usabiaga, G., Bocchetta, M., Van Leemput, K., Greve, D. N., Van der Kouwe, A., Fischl, B., Caballero-Gaudes, C., Paz-Alonso, P.M., 2018. A probabilistic atlas of the human thalamic nuclei combining ex vivo MRI and histology. Neuroimage 183, 314–326.
Johnston, R., Pitchford, N.J., Roach, N.W., Ledgeway, T., 2017. New insights into the role of motion and form vision in neurodevelopmental disorders. Neurosci. Biobehav. Rev. 83, 32–45.
JONES, D., 2008. Studying connections in the living human brain with diffusion MRI. Cortex 44 (8), 936–952.
Jones, D.K., Knosche, T.R., Turner, R., 2013. White matter integrity, fiber count, and other fallacies: the do's and don'ts of diffusion MRI. Neuroimage 73, 239–254.
Keller, S.S., Gerdes, J.S., Mohammadi, S., Kellinghaus, C., Kugel, H., Deppe, K., Ringelstein, E.B., Evers, S., Schwindt, W., Deppe, M., 2012. Volume estimation of the thalamus using freesurfer and stereology: consistency between methods. Neuroinformatics 10 (4), 341–350.
Kim, J.-N., Shadlen, M.N., 1999. Neural correlates of a decision in the dorsolateral prefrontal cortex of the macaque. Nat. Neurosci. 2 (2), 176–185.
Lam, F.C., Lovett, F., Dutton, G.N., 2010. Cerebral visual impairment in children: a longitudinal case study of functional outcomes beyond the visual acuities. J. Vis. Impair. Blindness 104 (10), 625–635.
Lennartsson, F., Nilsson, M., Flodmark, O., Jacobson, L., 2014. Damage to the immature optic radiation causes severe reduction of the retinal nerve fiber layer, resulting in predictable visual field defects. Invest. Ophthalmol. Vis. Sci. 55 (12), 8278–8288.
Macintyre-Beon, C., Ibrahim, H., Hay, I., Cockburn, D., Calvert, J., Dutton, G.N., Bowman, R., 2010. Dorsal stream dysfunction in children: a review and an approach to diagnosis and management. Curr. Pediatr. Rev. 6 (3), 166–182.
Macintyre-Béon, C., Young, D., Dutton, G.N., Mitchell, K., Simpson, J., Loffler, G., Bowman, R., Hamilton, R., 2013. Cerebral visual dysfunction in prematurely born children attending mainstream school. Documenta ophthalmol. Adv. Ophthalmol. 127 (2), 89–102.
MacKay, T.L., Jakobson, L.S., Ellemberg, D., Lewis, T.L., Maurer, D., Casiro, O., 2005. Deficits in the processing of local and global motion in very low birthweight children. Neuropsychologia 43 (12), 1738–1748.
McDowell, N., Dutton, G.N., 2019. Hemianopia and features of balint syndrome following occipital lobe hemorrhage: identification and patient understanding have aided functional improvement years after onset. Case Rep. Ophthalmol. Med. 2019, 3864572.
Nakashima, Y., Yamaguchi, M.K., Kanazawa, S., 2019. Development of center-surround suppression in infant motion processing. Curr. Biol. 29 (18), 3059–3064 e3052.
Neubert, F.-X., Mars, R., Thomas, A., Sallet, J., Rushworth, M.S., 2014. Comparison of human ventral frontal cortex areas for cognitive control and language with areas in monkey frontal cortex. Neuron 81 (3), 700–713.
Ortibus, E., Verhoeven, J., Sunaert, S., Casteels, I., de Cock, P., Lagae, L., 2012. Integrity of the inferior longitudinal fasciculus and impaired object recognition in children: a diffusion tensor imaging study. Dev. Med. Child Neurol. 54 (1), 38–43.
Pavlova, M., Staudt, M., Sokolov, A., Birbaumer, N., Krageloh-Mann, I., 2003. Perception and production of biological movement in patients with early periventricular brain lesions. Brain 126 (3), 692–701.
Philip, S.S., Dutton, G.N., 2014. Identifying and characterising cerebral visual impairment in children: a review. Clin. Exp. Optom. 97 (3), 196–208.
Pitzalis, S., Galletti, C., Huang, R.-S., Patria, F., Committeri, G., Galati, G., Fattori, P., Sereno, M.I., 2006. Wide-field retinotopy defines human cortical visual area v6. J. Neurosci. 26 (30), 7962–7973.
Previc, F.H., Liotti, M., Blakemore, C., Beer, J., Fox, P., 2000. Functional imaging of brain areas involved in the processing of coherent and incoherent wide field-of-view visual motion. Exp. Brain Res. 131 (4), 393–405.
Putcha, D., Ross, R.S., Rosen, M.L., Norton, D.J., Cronin-Golomb, A., Somers, D.C., Stern, C.E., 2014. Functional correlates of optic flow motion processing in Parkinson's disease. Front. Integr. Neurosci. 8, 57.
Royden, C.S., 2002. Computing heading in the presence of moving objects: a model that uses motion-opponent operators. Vision Res. 42 (28), 3043–3058.
Sakki, H.E.A., Dale, N.J., Sargent, J., Perez-Roche, T., Bowman, R., 2018. Is there consensus in defining childhood cerebral visual impairment? A systematic review of terminology and definitions. Br. J. Ophthalmol. 102 (4), 424–432.
Sallet, J., Mars, R.B., Noonan, M.P., Neubert, F.-X., Jbabdi, S., O'Reilly, J.X., Filippini, N., Thomas, A.G., Rushworth, M.F., 2013. The organization of dorsal frontal cortex in humans and macaques. J. Neurosci. 33 (30), 12255–12274.
Schallmo, M.P., Kale, A.M., Millin, R., Flevaris, A.V., Brkanac, Z., Edden, R.A., Bernier, R. A., Murray, S.O., 2018. Suppression and facilitation of human neural responses. eLife 7, e30334.
Schallmo, M.P., Kolodny, T., Kale, A.M., Millin, R., Flevaris, A.V., Edden, R.A.E., Gerdts, J., Bernier, R.A., Murray, S.O., 2020. Weaker neural suppression in autism. Nat. Commun. 11 (1), 2675.
Schmidt, C., Plickert, S., Summers, D., Zerr, I., 2010. Pulvinar sign in Wernicke's encephalopathy. CNS Spectr. 15 (4), 215–219.
Seiffert, A.E., Somers, D.C., Dale, A.M., Tootell, R.B., 2003. Functional MRI studies of human visual motion perception: texture, luminance, attention and after-effects. Cereb. Cortex 13 (4), 340–349.
Sherrill, K.R., Chrastil, E.R., Ross, R.S., Erdem, U.M., Hasselmo, M.E., Stern, C.E., 2015. Functional connections between optic flow areas and navigationally responsive brain regions during goal-directed navigation. Neuroimage 118, 386–396.
Sincich, L.C., Park, K.F., Wohlgemuth, M.J., Horton, J.C., 2004. Bypassing V1: a direct geniculate input to area MT. Nat. Neurosci. 7 (10), 1123–1128.
Smith, A.T., Wall, M.B., Williams, A.L., Singh, K.D., 2006. Sensitivity to optic flow in human cortical areas MT and MST. Eur. J. Neurosci. 23 (2), 561–569.
Solebo, A.L., Teoh, L., Rahi, J., 2017. Epidemiology of blindness in children. Arch. Dis. Child. 102 (9), 853–857.
Somers, D.C., Todorov, E.V., Siapas, A.G., Toth, L.J., Kim, D.S., Sur, M., 1998. A local circuit approach to understanding integration of long-range inputs in primary visual cortex. Cereb. Cortex 8 (3), 204–217.
Song, S.-K., Sun, S.-W., Ramsbottom, M.J., Chang, C., Russell, J., Cross, A.H., 2002. Dysmyelination revealed through MRI as increased radial (but unchanged axial) diffusion of water. Neuroimage 17 (3), 1429–1436.
Tadin, D., 2015. Suppressive mechanisms in visual motion processing: From perception to intelligence. Vision Res. 115 (Pt A), 58–70.
Tadin, D., Lappin, J.S., Gilroy, L.A., Blake, R., 2003. Perceptual consequences of centre-surround antagonism in visual motion processing. Nature 424 (6946), 312–315.
Tadin, D., Kim, J., Doop, M.L., Gibson, C., Lappin, J.S., Blake, R., Park, S., 2006. Weakened center-surround interactions in visual motion processing in schizophrenia. J. Neurosci. 26 (44), 11403–11412.
Tadin, D., Park, W.J., Dieter, K.C., Melnick, M.D., Lappin, J.S., Blake, R., 2019. Spatial suppression promotes rapid figure-ground segmentation of moving objects. Nat. Commun. 10 (1), 2732.

Takahashi, S., Yonezawa, H., Takahashi, J., Kudo, M., Inoue, T., Tohgi, H., 2002. Selective reduction of diffusion anisotropy in white matter of Alzheimer disease brains measured by 3.0 Tesla magnetic resonance imaging. Neurosci. Lett. 332 (1), 45–48.

Taylor, N.M., Jakobson, L.S., Maurer, D., Lewis, T.L., 2009. Differential vulnerability of global motion, global form, and biological motion processing in full-term and preterm children. Neuropsychologia 47 (13), 2766–2778.

Thiebaut de Schotten, M.T., Dell'Acqua, F., Forkel, S.J., Simmons, A., Vergani, F., Murphy, D.G.M., Catani, M., 2011. A lateralized brain network for visuospatial attention. Nat. Neurosci. 14 (10), 1245–1246.

Tootell, R.B.H., Mendola, J.D., Hadjikhani, N.K., Ledden, P.J., Liu, A.K., Reppas, J.B., Sereno, M.I., Dale, A.M., 1997. Functional analysis of V3A and related areas in human visual cortex. J. Neurosci. 17 (18), 7060–7078.

Tootell, R.B., Reppas, J.B., Kwong, K.K., Malach, R., Born, R.T., Brady, T.J., Rosen, B.R., Belliveau, J.W., 1995. Functional analysis of human MT and related visual cortical areas using magnetic resonance imaging. J. Neurosci. 15 (4), 3215–3230.

Toth, L.J., Rao, S.C., Kim, D.S., Somers, D., Sur, M., 1996. Subthreshold facilitation and suppression in primary visual cortex revealed by intrinsic signal imaging. Proc. Natl. Acad. Sci. USA 93 (18), 9869–9874.

Turkozer, H.B., Pamir, Z., Boyaci, H., 2016. Contrast affects fMRI activity in middle temporal cortex related to center-surround interaction in motion perception. Front. Psychol. 7, 454.

van Genderen, M., Dekker, M., Pilon, F., Bals, I., 2012. Diagnosing cerebral visual impairment in children with good visual acuity. Strabismus 20 (2), 78–83.

VerMaas, J.R., Gehringer, J.E., Wilson, T.W., Kurz, M.J., 2019. Children with cerebral palsy display altered neural oscillations within the visual MT/V5 cortices. Neuroimage Clin. 23, 101876.

Volpe, J.J., 2009. Brain injury in premature infants: a complex amalgam of destructive and developmental disturbances. Lancet Neurol. 8 (1), 110–124.

Weinstein, J.M., Gilmore, R.O., Shaikh, S.M., Kunselman, A.R., Trescher, W.V., Tashima, L.M., Boltz, M.E., McAuliffe, M.B., Cheung, A., Fesi, J.D., 2012. Defective motion processing in children with cerebral visual impairment due to periventricular white matter damage. Dev. Med. Child Neurol. 54 (7), e1–e8.

Wetherill, G.B., Levitt, H., 1965. Sequential estimation of points on a psychometric function. Br. J. Math. Stat. Psychol. 18, 1–10.

Yeh, F.C., Tseng, W.Y., 2013. Sparse solution of fiber orientation distribution function by diffusion decomposition. PLoS ONE 8 (10), e75747.

Yeh, F.C., Wedeen, V.J., Tseng, W.Y., 2010. Generalized q-sampling imaging. IEEE Trans. Med. Imaging 29 (9), 1626–1635.

Zeki, S., Watson, J.D., Lueck, C.J., Friston, K.J., Kennard, C., Frackowiak, R.S., 1991. A direct demonstration of functional specialization in human visual cortex. J. Neurosci. 11 (3), 641–649.

Zenger-Landolt, B., Heeger, D.J., 2003. Response suppression in v1 agrees with psychophysics of surround masking. J. Neurosci. 23 (17), 6884–6893.